

# Quantitative Architecture Distinguishes Prefrontal Cortical Systems in the Rhesus Monkey

S.M. Dombrowski, C.C. Hilgetag<sup>1</sup> and H. Barbas<sup>1,2,3</sup>

Departments of Behavioral Neuroscience and <sup>1</sup>Anatomy and Neurobiology, Boston University School of Medicine, Boston, MA, <sup>2</sup>Department of Health Sciences, Boston University, 635 Commonwealth Ave., #431, Boston MA, 02218 and <sup>3</sup>New England Regional Primate Research Center, Harvard Medical School, Boston, MA, USA

The prefrontal cortex encompasses a large and heterogeneous set of areas, whose borders have been variously mapped in different architectonic studies. Differences in cortical maps present a formidable problem in comparing data across studies and in constructing databanks on the connections and functional attributes of cortical areas. Here we used quantitative approaches to cortical mapping to investigate (i) if architectonic areas of the prefrontal cortex in adult rhesus monkeys have unique profiles and (ii) if groups of architectonic areas belonging to distinct cortical types, ranging from agranular to eulaminar, have similar features. In addition, we used multidimensional analyses to see if, and how, prefrontal areas form clusters when multiple features are considered simultaneously. We used quantitative unbiased sampling procedures to estimate the areal and laminar density of neurons, glia and neurons positive for the calcium binding proteins parvalbumin (PV), calbindin (CB) and calretinin (CR) among 21 prefrontal areas or subdivisions of areas. Neuronal density varied among the prefrontal cortices (range:  $38\,569 \pm 4078$  to  $58\,708 \pm 2327$  neurons/mm<sup>3</sup>); it was lowest in caudal orbitofrontal and medial areas (OPAll, OPro, 13, 24a, 32, M25) and highest in lateral prefrontal areas (subdivisions of areas 46 and 8). Neurons positive for PV were most prevalent in lateral prefrontal areas and least prevalent in caudal orbitofrontal and medial prefrontal areas, whereas the opposite trend was noted for neurons that expressed CB. Neurons positive for CR did not show regional differences, and the density of glia showed small variations among prefrontal cortices. The differences among areas, along with differences in the thickness of individual areas and layers, were used to establish a quantitative profile for each area. The results showed that differences in the density of neurons, and the preponderance of neurons positive for PV and CB, were related to different architectonic types of areas found within the prefrontal cortex. Conventional as well as multi-parameter statistical analyses distinguished at one extreme the agranular and dysgranular (limbic) cortices, which were characterized by prominent deep layers (V–VI), the lowest neuronal density, the highest ratio of glia/neurons, and the lowest density of PV and the highest for CB. At the other extreme, lateral eulaminar cortices were characterized by the highest density of neurons, a prominent granular layer IV, denser supragranular (II–III) than infragranular (V–VI) layers, and a balanced distribution of neurons positive for PV and CB. The results provide insights into potentially different rates of development or maturation of limbic and eulaminar prefrontal areas, and their differential vulnerability in neurological and psychiatric diseases. The quantitative methods used provide an objective approach to construct maps, address differences in nomenclature across studies, establish homologies in different species and provide a baseline to identify changes in pathologic conditions.

## Introduction

The prefrontal cortex in primates extends from the frontal pole to the premotor cortex, and is composed of several heterogeneous areas identified in classic architectonic studies (Brodmann, 1905; Vogt and Vogt, 1919; Walker, 1940; Von Bonin and Bailey, 1947; Sanides, 1970). Structural differences may underlie the

role of distinct prefrontal cortices in complex cognitive, mnemonic and emotional processes [for reviews see (Goldman-Rakic, 1988; Petrides, 1989; Fuster, 1989, 1993; Barbas, 1995)]. Architectonic areas of the prefrontal cortex in macaque monkeys, first mapped on the basis of cellular features, and the distribution of myelin (Brodmann, 1905; Vogt and Vogt, 1919; Walker, 1940; Von Bonin and Bailey, 1947; Sanides, 1970; Barbas and Pandya, 1989; Preuss and Goldman-Rakic, 1991; Morecraft *et al.*, 1992) have been subdivided further with the aid of modern cellular and molecular stains [e.g. (Hof and Nimchinsky, 1992; Carmichael and Price, 1994; Nimchinsky *et al.*, 1996)]. However, architectonic studies rely on qualitative differences in a number of morphological cellular and neurochemical features among areas, which may account for disagreements in areal subdivisions. Differences in maps and nomenclature present a formidable problem in constructing central databanks on the connections and functional attributes of areas obtained from different studies (Stephan *et al.*, 2000).

In this study we used an alternative approach to cortical mapping by investigating whether architectonic areas of the prefrontal cortex can be characterized by a set of quantitative criteria. Architectonic areas vary in a number of laminar, cellular and molecular features. Here we focused on fundamental architectonic criteria that form the basis of classic architectonic studies, namely, density of neurons and glia, as well as some neurochemical markers for calcium binding proteins, which label distinct classes of cortical neurons and have proved valuable in architectonic studies [e.g. (Jones *et al.*, 1995; Gabbott and Bacon, 1996b)]. We asked the following questions. Do architectonic areas of the prefrontal cortex have unique profiles that can be described and illustrated quantitatively? Conversely, do groups of architectonic areas have similar features that may suggest common functions? We addressed the latter question in two ways. First, we tested whether areas belonging to distinct cortical types have similar features, according to the structural model of the prefrontal cortex (Barbas and Rempel-Clower, 1997). Unlike architectonic parcellation, which is based on the detailed cellular and molecular features of areas, cortical type relies on broad structural features shared by more than one architectonic area, including the number and distinction of identifiable layers. In the prefrontal cortex we previously identified several types of cortices, ranging from agranular, which have only three identifiable layers, to eulaminar, which have six distinct layers. The significance of cortical type is based on our previous findings indicating that the pattern of cortico-cortical connections can be predicted on the basis of the broad laminar features of the interconnected areas [e.g. (Barbas, 1986; Barbas and Rempel-Clower, 1997; Rempel-Clower and Barbas, 2000)]. In a second approach, we used multidimensional analyses to see if, and how, prefrontal areas form clusters when multiple features are considered simultaneously. The latter

approach explored the structural similarities and differences of prefrontal areas independent of cortical type. The study of even a few architectonic features within the context of the complex areal and laminar features of the prefrontal cortex provided up to 18 parameter dimensions. The quantitative approaches to cortical architecture provided key insights that may justify the use of similar approaches to cortical mapping to begin to resolve differences in nomenclature across studies, establish homologies in different species and provide a baseline to identify changes in pathologic conditions [e.g. (O'Kusky and Colonnier, 1982; Selemon *et al.*, 1995, 1998; Gabbott and Bacon, 1996b)].

## Materials and Methods

### Tissue Processing

Data were obtained from seven adult rhesus monkeys (*Macaca mulatta*). Seven animals were used to estimate the regional density of neurons and glia, and five of these were used to study the distribution of the calcium binding proteins parvalbumin (PV), calbindin (CB) and calretinin (CR). Experimental procedures were conducted according to the *NIH Guide for the Care and Use of Laboratory Animals* (NIH publication #86-23, revised 1987).

### Perfusion and Cryoprotection

Animals were given an overdose of anesthetic (sodium pentobarbital) and perfused through the heart with saline, followed by 2 l of fixative (4% paraformaldehyde in 0.1 M phosphate buffer, pH 7.4). The brain was removed from the skull, photographed and cryoprotected in graded solutions of sucrose (12, 16, 20 and 30%). The brain was then frozen in  $-70^{\circ}\text{C}$  isopentane according to Rosene and Rhodes (Rosene and Rhodes, 1990), cut on a freezing microtome in the coronal plane at  $40\ \mu\text{m}$  in 10 series and collected in 0.1 M phosphate buffer.

### Nissl Staining

One series of sections was stained for Nissl using either thionin or cresyl violet to identify neurons and glia, and to delineate architectonic borders (Ling and Leblond, 1973; Ling *et al.*, 1973; Gabbott and Stewart, 1987; Barbas and Pandya, 1989). Nissl staining using thionin (five cases) and cresyl violet (two cases) yielded similar results. Sections mounted on chrome-alum coated slides were dried, defatted in a 1:1 solution of chloroform and 100% ethanol for 1 h, rehydrated through a series of graded alcohols and  $\text{dH}_2\text{O}$ , stained with 0.05% thionin (pH 4.5) or 0.1% cresyl violet (pH 3.8) for 3 min, differentiated through graded alcohols and xylenes, and coverslipped with Permount (Fisher Scientific, Springfield, NJ).

### Immunocytochemistry for PV, CB and CR

Matched series of sections were used for immunocytochemical staining of PV, CB, and CR. Antibodies for the calcium binding proteins were purchased from commercial sources (Swiss Antibodies, anti-PV #235, monoclonal; anti-CB D-28k #300, monoclonal; anti-CR #7696, polyclonal). Antibodies were specific for PV, CB and CR with no cross-reactivity (Celio *et al.*, 1988, 1990; Schwaller *et al.*, 1993). Free-floating sections were washed ( $3 \times 10$  min) in 0.1 M phosphate buffered saline (PBS, pH 7.4) and placed in 6% horse serum (PV and CB) or 6% goat serum (CR) for 1 h. They were then rinsed in 0.1 M PBS ( $3 \times 10$  min), placed in a 0.1 M PBS solution containing the antiserum for either PV, CB or CR (PV dilution 1:3000; CR and CB 1:2000) and incubated for 72 h at  $4^{\circ}\text{C}$  with gentle agitation. Sections were then rinsed ( $3 \times 10$  min) in 0.1 M PBS and processed for immunocytochemistry according to the instructions in the Vector ABC kit (Vector Labs, Burlingame, CA). Sections were placed in a 0.1 M PBS solution containing either anti-mouse IgG (PV and CB, Vector Labs BA-2000) or anti-rabbit IgG (CR, Vector Labs BA-1000) and incubated for 2 h at room temperature, then rinsed ( $3 \times 10$  min) in 0.1 M PBS and placed in the avidin-biotin-HRP complex for 90 min at room temperature. Sections were rinsed twice (10 min each) in 0.1 M PBS and once in 0.1 M PB (10 min), placed in a solution containing 0.05% 3,3'-diaminobenzidine (DAB) and 0.03% hydrogen peroxide in 0.1 M phosphate buffer for 3 min, then rinsed in 0.1 M PB ( $3 \times 10$  min) and mounted on chrome-alum

coated slides. A few sections were counterstained for Nissl to help delineate architectonic borders. Sections were dehydrated in graded series of alcohols and xylenes and coverslipped with Permount (Fisher Scientific). Control experiments were conducted in which the primary antibody was omitted while all other steps were identical to the experimental conditions.

### Prefrontal Areal and Laminar Boundaries

Twenty-one prefrontal areas or subdivisions of areas were investigated based on the architectonic map of Barbas and Pandya (Barbas and Pandya, 1989), modified from classic maps (Vogt and Vogt, 1919; Walker, 1940). Prefrontal cortices included medial areas 24a, 32, M25, M9, M10 and M14, orbitofrontal areas OPAll, OPro, area 13, area 11 and O12, and lateral areas 46 and 8. Areas 46 and 8 were further subdivided into their dorsal (D) and ventral (V) components. Areas 13 and 8 were subdivided into their gyral (g) and sulcal (s) parts. Areas 24a and 46, which extend almost along the entire rostrocaudal span of the prefrontal region, were divided into rostral, middle and caudal thirds. Only the rostral (r) and caudal (c) parts of areas 24a and 46 were included for analysis.

Neurons and glia were distinguished in Nissl stained sections by cell size and shape, and nuclear staining characteristics. Neurons were relatively large with a pale blue cytosol and clearly identified nucleolus, while glia were usually smaller with intensely stained nucleus. All glia, including astrocytes, oligodendrocytes and microglia, were placed in one category.

Prefrontal areas identified in Nissl stained sections were matched to corresponding sections stained for PV, CB and CR. The rostral and caudal limits of each area were identified through serial coronal sections. For each section architectonic boundaries were identified under a microscope (Nikon, Optiphot). Drawings of architectonic borders were transferred from the slides onto paper by means of a digital plotter (Hewlett Packard, 7475A) electronically coupled to the stage of the microscope and to a PC computer, as described previously [e.g. (Barbas *et al.*, 1999)]. The boundary of each area was plotted and stored on disc as a series of  $x$  and  $y$  coordinates.

Each prefrontal area was subdivided into laminar subgroups to allow comparison in density across areas. Layer I is easily distinguishable in all areas and made up one laminar subgroup. Layers II-III were included into one group as were layers V-VI because there is no clear distinction between each pair of layers in some prefrontal cortices (the agranular and dysgranular). For comparison, the same grouping was used for all prefrontal cortices. In most prefrontal areas layer IV was distinct and formed an additional group. Agranular (areas OPAll and 24a) and dysgranular (areas OPro, 13, M25, and 32) areas were subdivided into three laminar subgroups, (i) layer I, (ii) layers II-III and (iii) layers V-VI, because they either lack (agranular) or have only a rudimentary granular layer IV (dysgranular). In dysgranular areas an incipient and poorly defined layer IV was included with layers V and VI.

In sections stained for PV, CB and CR, areas were subdivided into two laminar subgroups, layers I-III and layers IV-VI, because it was not possible to parcel the cortex into finer laminar subgroups in unstained sections, where neuropile positive for the calcium binding proteins further obscured the fine laminar boundaries seen in Nissl stained sections.

### Counting Method

Laminar subgroups for each area were subdivided from coronal sections into counting boxes ( $50 \times 50\ \mu\text{m}$ , width  $\times$  height). This was accomplished using computer software to superimpose an electronic grid over an area and identify counting boxes by a series of  $x$  and  $y$  coordinates. The specific counting boxes used to gather data were selected randomly by a computer program. The stage was then positioned to the precise  $x$  and  $y$  coordinates of each counting box. Counting was performed through the optics of the microscope using a crosshair microgrid with known dimensions as reference.

The density of neurons and glia was estimated using a counting method adapted from previous studies (Sterio, 1984; Braendgaard and Gundersen, 1986; Williams and Rakic, 1988; Gundersen *et al.*, 1988; West and Gundersen, 1990; West, 1993) [for a review see (Coggeshall and Lekan, 1996)]. This method is based on the principle that each cell within a region of interest has an equal chance of being counted (West, 1993).

Neurons and glia were counted under a magnification of  $\times 1000$  under oil immersion. Counting methods followed specific three-dimensional ( $x$ , width;  $y$ , height; and  $z$ , thickness) inclusion/exclusion criteria to avoid the possibility of counting a cell more than once. As predetermined, the  $x$  and  $y$  exclusion criteria were defined as the left and frontal planes of each counting box. The  $z$  exclusion criterion was defined as the top plane of each counting box or the first object to come into focus (e.g. a neuron). Thus, neurons or glia touching or overlapping the left, frontal or top borders of the counting box were excluded from the counts, and those located exclusively within the counting box, or that crossed the right, back or bottom borders of the counting box were included in the counts and were recorded in a database. In Nissl stained sections neurons and glia were counted by nuclei, and in tissue processed for the calcium binding proteins by the cell body, as it was not possible to identify the nuclei in darkly labeled neurons in the latter.

Adequate sample size for analysis was determined using the formula of West *et al.* (West *et al.*, 1991)

$$CV^2 = ECV^2 + CE_{j-1}^2$$

which takes into consideration the coefficient of variance (CV), the coefficient of error (CE) and the expected coefficient of variance (ECV) to determine the optimal number of cases, sections and samples ( $j$ ) necessary for reliable estimates of cell density. Using this formula, we estimated that the minimum sampling size for this study was three cases, three sections and three samples per laminar subdivision. This minimum sample was exceeded in this study by using seven cases (five for PV, CB, CR), three sections and five samples for each laminar subgroup. The above formula yielded similar results when applied to two different samples stained for Nissl or PV.

The thickness of the cortex from pia to the white matter was measured for each prefrontal area by capturing images with a CCD camera (Dage) mounted on the microscope. The thickness of laminar subgroups was measured using image analysis software (MetaMorph, Universal Imaging Corp., Westchester, PA). Thickness measures were averaged from six cases, five sections in each case, and five measures in each section.

## Data Analysis

### Tissue Shrinkage

Whole brain volume was estimated by fluid immersion and displacement based on Archimedes' principle, before cryoprotection, and then sequentially after each time the brain sank in each upwardly graded concentration of sucrose. At the completion of cryoprotection in 30% sucrose there was a reduction of 30% in whole brain volume. Section thickness variation was  $<3\%$  for wet mounted sections cut at  $40\ \mu\text{m}$ , but shrinkage in the  $z$  dimension was considerable after air drying (50%), or in coverslipped sections treated to visualize calcium binding proteins (62%) or stained for Nissl (77%). In contrast, there was minimal shrinkage in the  $x$  and  $y$  dimensions in immunoreacted or Nissl stained sections (1–4%) in comparison with untreated wet mounted sections.

In order to compare densities of neurons and glia treated using several procedures, all measures were made on the basis of wet volume, so that section thickness was considered to be  $40\ \mu\text{m}$  with no correction factor for shrinkage. Because of the considerable and variable shrinkage in the  $z$  dimension, we did not apply a guard zone for the  $z$ -axis, with the caveat that there may be some error in the counts due to cell splitting or cell plucking (Williams and Rakic, 1988).

Density was initially obtained for each counting box as the number of neurons per unit volume ( $50 \times 50 \times 40\ \mu\text{m}$ , or  $10^{-4}\ \text{mm}^3$ ). Laminar density was calculated as the average density of all counting boxes within an individual laminar subgroup. Areal density was then calculated as the sum of laminar densities found within each architectonic area multiplied by the fraction of volume each laminar subgroup occupied in each area, and expressed as neurons/ $\text{mm}^3$ . Density values in each area and cortical thickness were used to estimate the number of neurons and glia in a three-dimensional cortical column under  $1\ \text{mm}^2$  of cortical surface, and to calculate the ratio of glia/neurons and the proportion of neurons positive for PV, CB and CR.

First and second order descriptive statistics were calculated to verify a

sufficiently normal distribution of the measures across cases of individual animals. Data are presented as the mean  $\pm$  SEM ( $SD/n^{1/2}$ ) for seven (neurons and glia) and five cases (PV, CB, and CR). Means were first compared using one-way analysis of variance (ANOVA) and then, if significantly different, by Scheffé post-hoc comparisons (STATISTICA, StatSoft, Inc.). Significant differences were set at a probability value of  $P < 0.05$ .

### Grouping Architectonic Areas According to Cortical Type

Using an approach based on broad structural features of the prefrontal cortex, we combined data into four categories: agranular, dysgranular, eulaminate I and eulaminate II. Categories were constructed on the basis of the number of layers and degree of laminar definition in each area. Agranular areas have three layers (areas OPaII and 24a) and dysgranular cortices have four layers (areas OPro, M25, 13 and 32). Eulaminate categories included granular cortices characterized by six layers. Orbital and medial granular cortices, which have a moderate degree of laminar definition, made up the 'eulaminate I' category (areas M9, M10, 11, O12 and M14). Lateral granular types of cortices that have the best laminar definition were included in the 'eulaminate II' category (areas 46 and 8).

### Multi-parameter Analyses

Using a different approach, we employed three distinct means of data analysis to assess global similarities and differences among prefrontal cortical areas, on the basis of the different morphological and cytological measures: (i) discriminant analysis (DA); (ii) nonmetric multidimensional scaling (NMDS); and (iii) hierarchical cluster analysis (HCA). The analyses were performed in SYSTAT V.10 for Windows (SPSS Inc.).

DA identifies those experimental measures that show the smallest overlap and clearest separation of the distributions of individual data points belonging to different entities (here, prefrontal cortices), i.e. those measures that are most informative and characteristic for the identification of all individual areas. DAs were carried out both for the experimental measures summed across all layers and for the same measures separated by lamina.

For the purpose of NMDS and cluster analyses, data were treated as normalized laminar profiles. That is, data were normalized for each cortical area by adding the respective measure (e.g. neuronal density, ND) across all layers and dividing each laminar feature by the sum, e.g.

$$ND[\text{layer I}]/\Sigma ND[\text{I, II-III, IV, V-VI}]$$

This analysis produced indicators for the relative laminar dominance of the different density measures or thickness across the cortical layers. To adjust degrees of freedom for subsequent correlation analyses, one of the relative laminar coordinates resulting from the normalization was omitted. This concerned the layer IV coordinate for the ND, glial density (GD) and cortical thickness (THI) measures and the IV-VI coordinate for the calcium binding protein (CPB) measures PV, CR and CB. Where measures were available for only the whole of an area, the description was assumed to hold for all of the area's subdivisions as well, to make measures available on the most detailed level of description. For instance, the data on cortical thickness distinguished between gyral and sulcal portions of area 13, whereas calcium binding data were only available for the area as a whole. Consequently, the same calcium binding density was assigned to both sub-divisions. As a result of this data conditioning process, each of the 21 areas or area subdivisions could be described with combinations of up to 12 laminar profiles from the different experimental measures [normalization of the original 18 laminar measures and adjustment of degrees of freedom as described above left the 12 measures: ND (I, II-III, V-VI); GD (I, II-III, V-VI); THI (I, II-III, V-VI); PV (I-III); CR (I-III); CB(I-III)], and analyses were based on the complete set, or on selected subsets, of these coordinates. Both NMDS and HCA investigations employed squared area (dis)similarity matrices derived from the normalized laminar profiles by Pearson's correlation.

NMDS (Kruskal, 1964) arranges areas in a chosen low-dimensional (typically two- or three-dimensional) space, based on the pairwise correlation (dis)similarities between the areas. The relative proximity between items in an NMDS diagram represents their relative similarity. The NMDS analyses used SYSTAT default settings with  $R$ -metric = 2, and

employing Guttman's (Guttman, 1968) coefficient of alienation for assessing the data's goodness of fit in two dimensions.

HCA hierarchically groups areas based on (dis)similarities in their parameter profiles, which are interpreted as spatial distances. The relative similarity of areas is expressed as the distance between two branching points in a cluster tree diagram; the longer the inter-branch distance, the more dissimilar the subgroups. Default settings for HCA were based on an  $R^2$  correlation between the parameters, computing the linkage distance between different clusters either as the average of all pairwise individual distances or as the centroid distance between the clusters' averaged centers.

## Results

### Distribution of Neurons in Areas and Layers

The pattern of distribution of neurons and glia in the various prefrontal areas was similar among cases. However, for a given

prefrontal area there were overall differences in density among cases, which may reflect individual variation among monkeys.

The 21 prefrontal areas investigated varied quantitatively by overall neuronal density, as shown in Figure 1 (the range was  $38\,569 \pm 4078$  to  $58\,708 \pm 2327$  neurons/mm<sup>3</sup>). The lowest density was recorded in medial areas 32 and 24a and caudal orbitofrontal areas OPAlI and OPro, and the highest was noted in the gyral part of ventral area 8 (Fig. 1). On the orbital surface there was an increase in density of neurons from caudal orbitofrontal areas (areas OPAlI and OPro) to rostral orbital areas (areas 13, O12, 11). Similarly, among medial prefrontal areas the density of neurons was lowest in area 32 and caudal area 24a, and highest in rostral areas M10 and M14. Among lateral prefrontal areas neuronal density was lowest in the sulcal part of dorsal area 8 (D8s) and highest in the gyral part of ventral area 8 (V8g).

Prefrontal areas varied by the distribution of neurons in

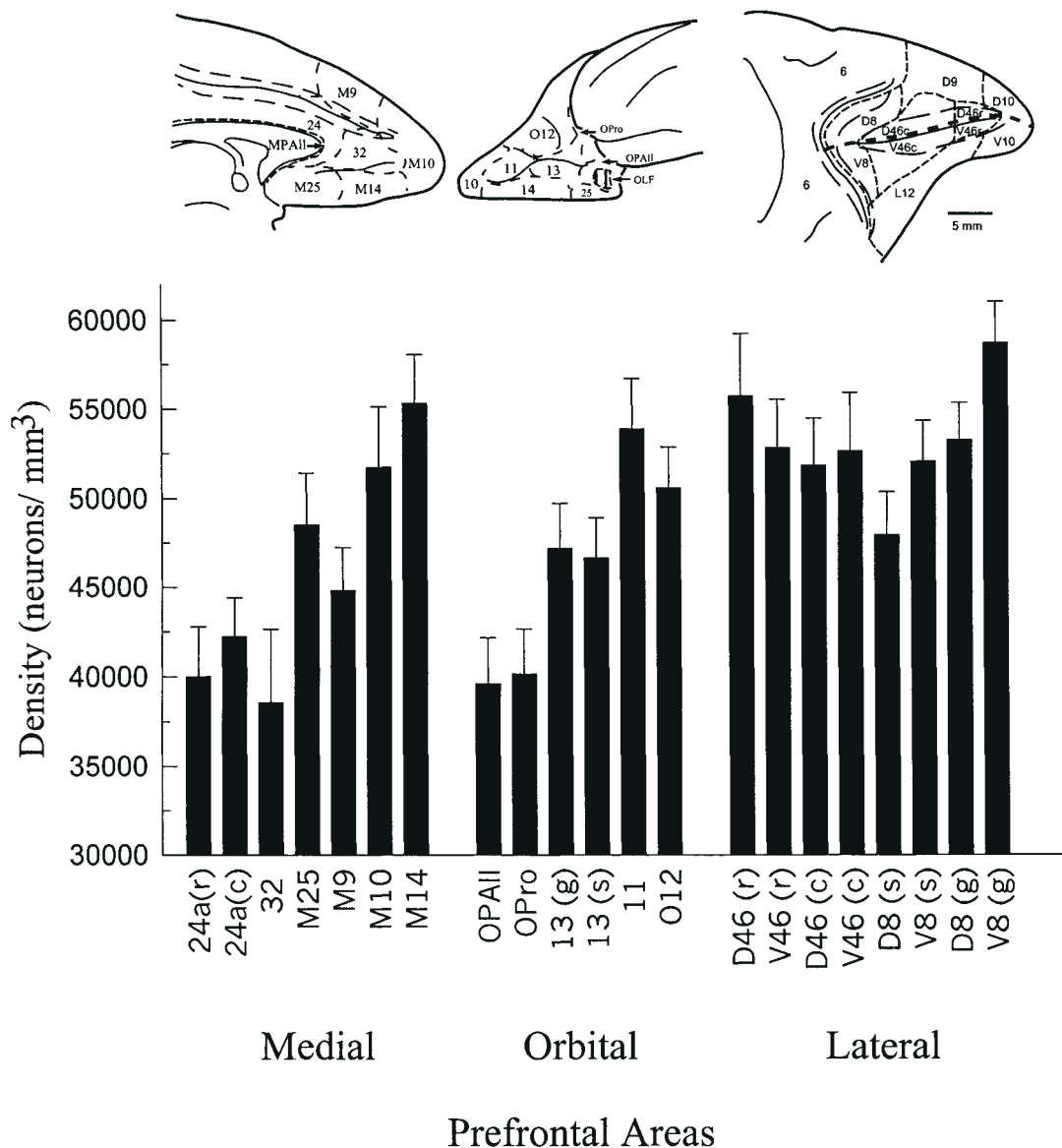


**Figure 1.** Density of neurons in 21 prefrontal areas or subdivisions of areas. Each bar represents the average density and standard error in seven cases. Density values for each area represent overall values measured across all cortical layers. A map of the prefrontal cortex above the bar graphs shows areas on the medial (left), orbital (center) and lateral (right) surfaces, adapted from the map of Walker (Walker, 1940) by Barbas and Pandya (Barbas and Pandya, 1989). Letters in connection with architectonic areas (designated by numbers) represent: C, caudal; D, dorsal; g, gyral; M, medial; O, orbital; R, rostral; s, sulcal; V, ventral.

different layers. In all areas layer I had the lowest density of neurons, and layer IV, when present, had the highest density (Fig. 2). In addition to general differences in laminar characteristics, architectonic areas have distinct laminar profiles. Areas 25 and 14, for example, were distinguished from all other prefrontal areas by a high cellular density in layers V and VI (Fig. 2D). Rostral area 24a differed from its caudal counterpart by having considerably higher cellular density in layers II and III in the latter (Fig. 1). The gyral part of area 8 stood apart from the sulcal part of area 8, and from other prefrontal areas by a higher overall density of neurons (Fig. 1).

A quantitative architectonic profile of each area emerged more clearly by combining the cellular density and cortical thickness for each area and layers (Fig. 3), yielding an estimate of the number of neurons situated below each square millimeter of cortical surface in a three-dimensional column. The lowest numbers of neurons under 1 mm<sup>2</sup> of pial surface were found in the caudal part of area 24a (66 582 ± 3441), area OPAll (70 857 ± 4575) and area 32 (74 284 ± 7854), and the highest were in the gyral part of area 13 (135 863 ± 7387) and the gyral part of ventral area 8 (128 042 ± 5075). Further, this analysis revealed that whereas orbital areas OPro and 13 have overall lower cell density than lateral areas 46 and 8, they have a comparable or higher overall number of neurons under 1 mm<sup>2</sup> of cortical surface on account of their greater thickness from pia to white matter (Fig. 3). The average number of neurons under 1 mm<sup>2</sup> of cortical surface was comparable for orbital (97 753 ± 5338) and lateral (97 560 ± 4801) areas, and was somewhat lower for medial areas (83 195 ± 5428).

#### Density of Neurons among Different Types of Prefrontal Cortices

Groups of areas belonging to different architectonic types differed significantly in neuronal density [ $F(3,17) = 12.59$ ,  $P < 0.01$ ], and the differences could be traced to a significant divergence between either eulaminate group and agranular and dysgranular areas, respectively ( $P < 0.05$ ). Neuronal density did not differ significantly between agranular and dysgranular cortices, or between eulaminate I and II cortices. Further analyses revealed that the four types of cortices differed significantly in neuronal density for layers II–III [ $F(3,17) = 22.63$ ,  $P < 0.01$ ], and Scheffé post-hoc comparisons indicated that eulaminate I or II areas had significantly higher neuronal density in layers II–III than either agranular or dysgranular cortices ( $P < 0.05$ ). The four types of prefrontal areas did not vary in neuronal density in layer I, layers V–VI or layer IV between eulaminate I and eulaminate II cortices.

Laminar group profiles that included information on density by layer and laminar thickness indicated that agranular and dysgranular areas were characterized by prominent layers V–VI (Fig. 4A,B, blue). By contrast, eulaminate cortices were distinguished by a well defined and dense layer IV (Fig. 4C,D, red). A higher cellular density in the upper layers was seen for the first time in eulaminate II cortices, which also had the highest cell density in layer IV among prefrontal cortices (Fig. 4D, green).

#### Distribution of Glia in Prefrontal Areas and Ratio of Glia/Neurons

There were some differences in the areal distribution of glia as well (the range was 43 128 ± 2748 to 56 534 ± 3607 glia/mm<sup>3</sup>). For example, glia were less densely distributed in medial areas M25, M14 and 32 and the orbitofrontal areas OPro and O12, and were more densely distributed in areas 46(c) and 8(s). Among cortical layers, glia were most prevalent in layer I, followed by

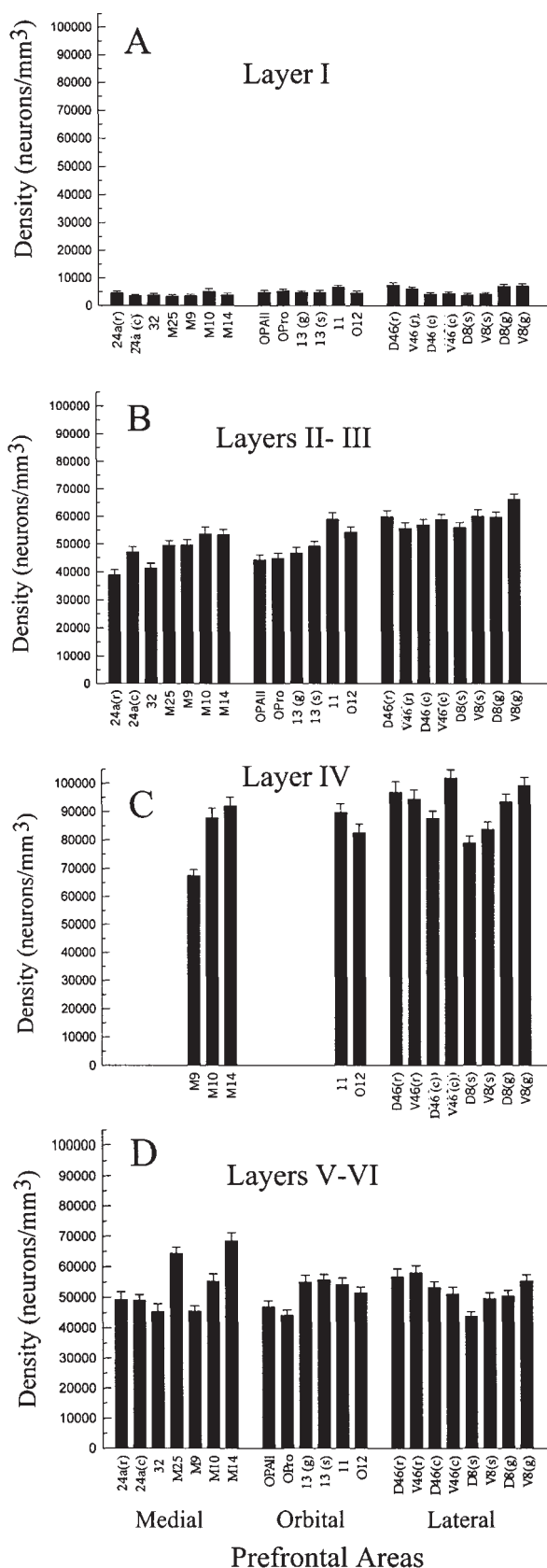


**Figure 2.** Density of neurons in prefrontal areas for laminar subgroups: (A) layer I; (B) layers II–III; (C) layer IV; (D) layers V–VI. The boundary of a rudimentary layer IV was not clearly distinguishable in dysgranular areas 32, M25, 13 and OPro, and was included with layers V–VI for these areas. Each bar represents the average neuronal density and standard error from seven cases.

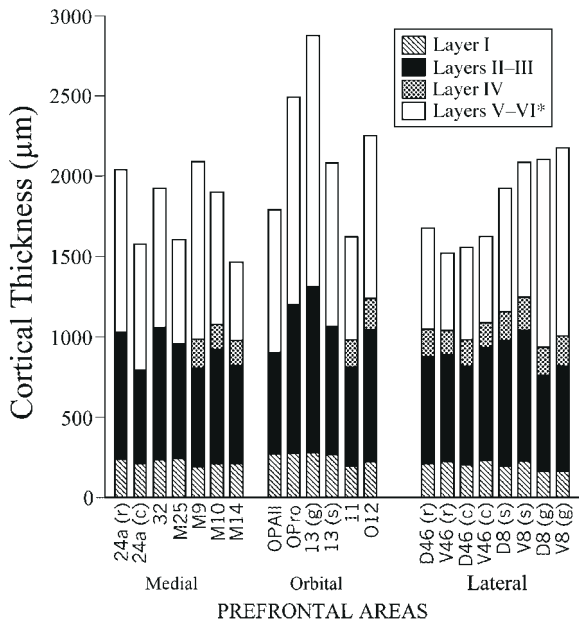


**Figure 3.** Cortical thickness of different layers in prefrontal areas. A rudimentary layer IV in dysgranular areas 32, M25, 13 and OPro was not clearly distinguishable, and was included with layers V–VI. Each bar represents the average cortical thickness from five sections in each of six cases.

layers V–VI and layer IV, and were least prevalent in layers II–III for all prefrontal cortices. Analysis by cortical type showed overall differences [ $F(3,17) = 9.15, P < 0.01$ ], and post-hoc comparisons showed that glia were significantly more densely distributed in eulaminate II than in either eulaminate I or dysgranular areas ( $P < 0.05$ ), but not agranular areas.

The above analysis indicated a small variation in the prevalence of glia among prefrontal cortices, but because areas varied considerably in neuronal density, so did the ratio of glia to neurons for areas (Fig. 5A) and for different types of cortices (Fig. 5B). In the latter, the average was higher in agranular than in other cortices (Fig. 5B), though the differences among all types were not statistically significant.

#### Calcium Binding Proteins: Distribution and Density

In all prefrontal areas the greatest concentration of PV positive neurons appeared in the middle cortical layers, corresponding to the deep part of layer III, layer IV and the upper part of layer V, while fewer positive neurons were found in layers II and VI. The density of PV positive neurons varied substantially in prefrontal cortices (the range was  $2497 \pm 600$  to  $8359 \pm 1100$  neurons/mm<sup>3</sup>), being lowest in medial areas 24a and M25 and caudal orbitofrontal areas OPAl and OPro, and highest in lateral areas 46, 8, and M9 (Fig. 6A).

CB positive neurons were found in all layers, but were most prevalent in two horizontal bands: a densely staining superficial

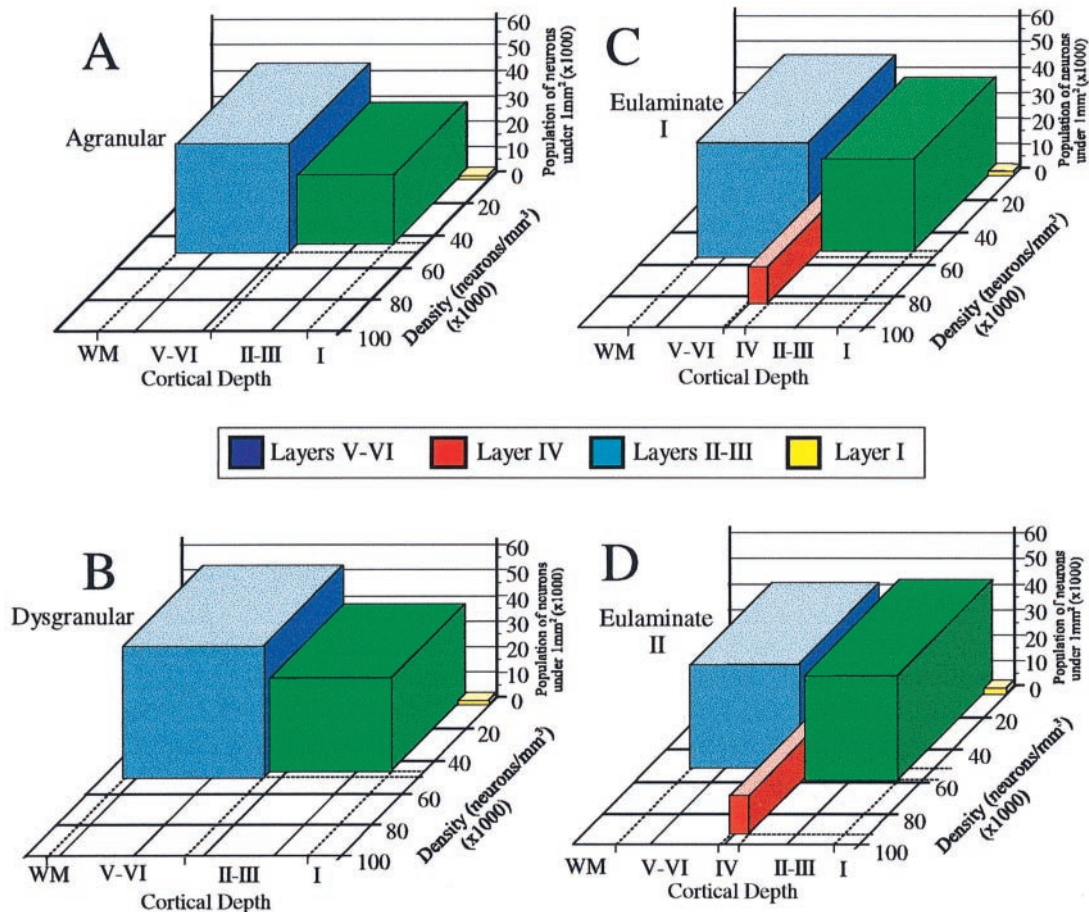


**Figure 4.** Neuronal density profile in different types of prefrontal cortices. Three-dimensional graphs showing differences in neuronal density (y-axis), laminar thickness by layer (x-axis) and number of neurons under 1 mm<sup>2</sup> of cortical surface (z-axis) in: (A) agranular, (B) dysgranular, (C) eulaminate I and (D) eulaminate II cortices. Dotted lines for the x-axis demarcate extent of cortical layers, and solid lines indicate 500 µm intervals of cortical thickness.

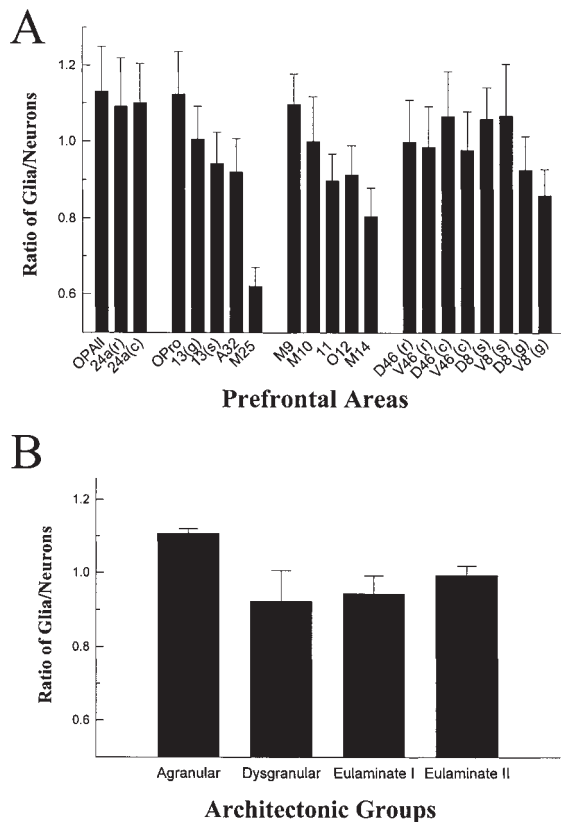


**Figure 5.** The relationship of glia to neurons in prefrontal cortices. (A) The ratio of glia/neurons in prefrontal areas or subdivisions of areas. (B) Variation in the ratio of glia/neurons in different types of cortices.

band corresponded to layers II-III, which had 2-3 times more positive neurons than a deep band corresponding to layers V-VI. CB positive neurons were seen only sparsely in layer I and in the white matter. Most CB positive neurons were non-pyramidal in shape. Larger, pyramidal CB positive neurons were noted in layers III and V, as reported previously (Condé *et al.*, 1994; Gabbott and Bacon, 1996a). The density of CB positive neurons ranged from  $5769 \pm 865$  to  $15\,140 \pm 1798$  neurons/mm<sup>3</sup>; it was lowest in medial area 9, caudal area 46 and area 8, and highest in caudal orbitofrontal areas (OPAll, OPro, 13) and area M25 (Fig. 6B).

CR positive neurons were concentrated in layer II, the deep part of layer I and the upper part of layer III. The deep cortical layers (IV-VI) had substantially fewer CR positive neurons. Overall, the range and average density of CR positive neurons was similar among prefrontal cortices, with the exception of area 24a, where the density was lower (Fig. 6C).

#### Density and Proportion of PV, CB and CR Positive Neurons in Different Types of Cortices

There were differences in PV positive neurons among the various types of prefrontal cortices [ $F(3,14) = 18.35$ ,  $P < 0.01$ ], as well as for CB [ $F(3,14) = 4.75$ ,  $P < 0.05$ ], which could be specifically traced to significant differences between both types of eulaminate cortices and agranular and dysgranular areas, respectively (for PV,  $P < 0.05$ ), or between dysgranular and eulaminate II areas (for CB,  $P < 0.05$ ). Agranular and dysgranular cortices had the highest density of CB positive neurons and the lowest for PV, where CB neurons outnumbered the PV by

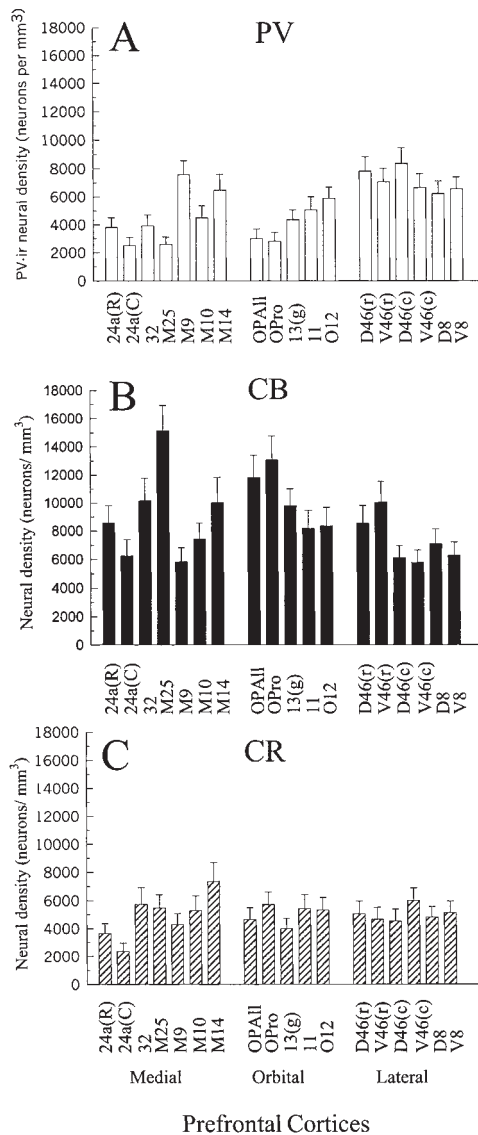


**Figure 6.** The density of calcium binding proteins in prefrontal cortices. (A) Parvalbumin (PV); (B) calbindin (CB); (C) calretinin (CR). Each bar represents the average density and standard error from five cases.

threefold. In contrast, in eulaminate cortices, the density of PV and CB neurons was similar (Fig. 7). In eulaminate I areas CB positive neurons were still more prevalent than PV positive ones, showing a distribution between that of the agranular/dysgranular areas, on the one hand, and that of the eulaminate II areas, on the other. CR positive neurons showed a relatively uniform distribution across prefrontal areas (Fig. 7).

Neurons positive for PV, CB and CR represent largely non-overlapping populations (Hendry *et al.*, 1989; van Brederode *et al.*, 1990; Kubota *et al.*, 1994; Gonchar and Burkhalter, 1997), and were considered as separate subpopulations. We expressed the density of PV, CB and CR positive neurons as a proportion of the population of neurons stained for Nissl in a three-dimensional column under 1 mm<sup>2</sup> of cortical surface. This new density analysis showed that neurons positive for the calcium binding proteins accounted for 36-50% of all neurons, and constituted a higher proportion in agranular and dysgranular cortices (44-50%) than in eulaminate cortices (36-37%). Overall, CB

positive neurons accounted for ~13–29% of the population of neurons, and PV and CR positive neurons accounted for 8–13 and 10–12%, respectively. In all areas PV, CB and CR represented a significantly higher proportion of the neuronal population in layers I–III than in layers IV–VI ( $P < 0.01$ ).

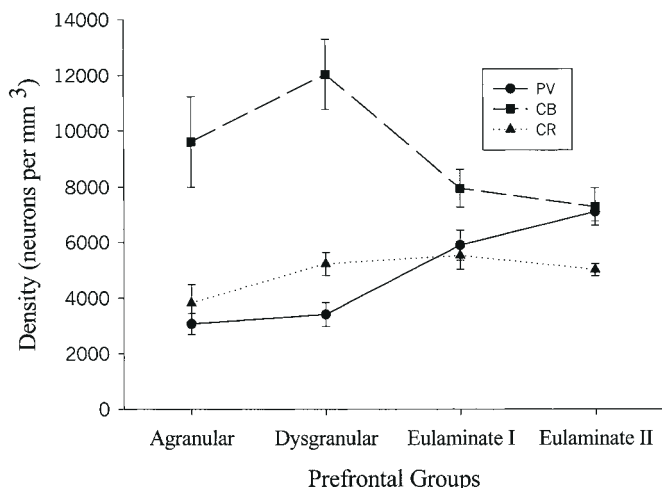


**Figure 7.** Differences in the density of CB and PV (but not CR) in different types of prefrontal cortices. The density of PV positive neurons was lowest in agranular and dysgranular cortices and highest in eulaminate I and II cortices, while the reverse was seen for CB.

## Global Structure of Prefrontal Cortex

### Specificity of Experimental Measures

At the outset of the statistical investigations of global prefrontal organization, a DA was performed to assess which of the six available experimental measures would be most specific for characterizing prefrontal cortices. This is equivalent to identifying the measures that showed the least overlap among areas in the individual data points. Considering the experimental measures summed across all layers, a backward DA determined ND, THI and PV as the most informative of the six available variables (Fig. 8), producing  $F$  values (the relative measure of freedom in the case of removing a variable from the set of all measures) of 12.84, 5.85 and 2.49, respectively. The ND measure in particular led to a noticeable separation of the data points belonging to different areas, also resulting in an apparent arrangement of the areas in at least two, and potentially three, clusters.

The DA was repeated taking into account the same measures separated by cortical layers, yielding a total of 18 independent measures (four layer measures each for ND, GD and THI, as well as two measures each for PV, CB and CR). When layer IV information in the ND, GD and THI measures for agranular and dysgranular areas was defined as missing, in order to avoid dominance by this highly distinctive layer, THI of layers V–VI, THI I and PV IV–VI were the most informative measures (producing  $F$  values of 14.99, 3.41 and 2.63, respectively). In

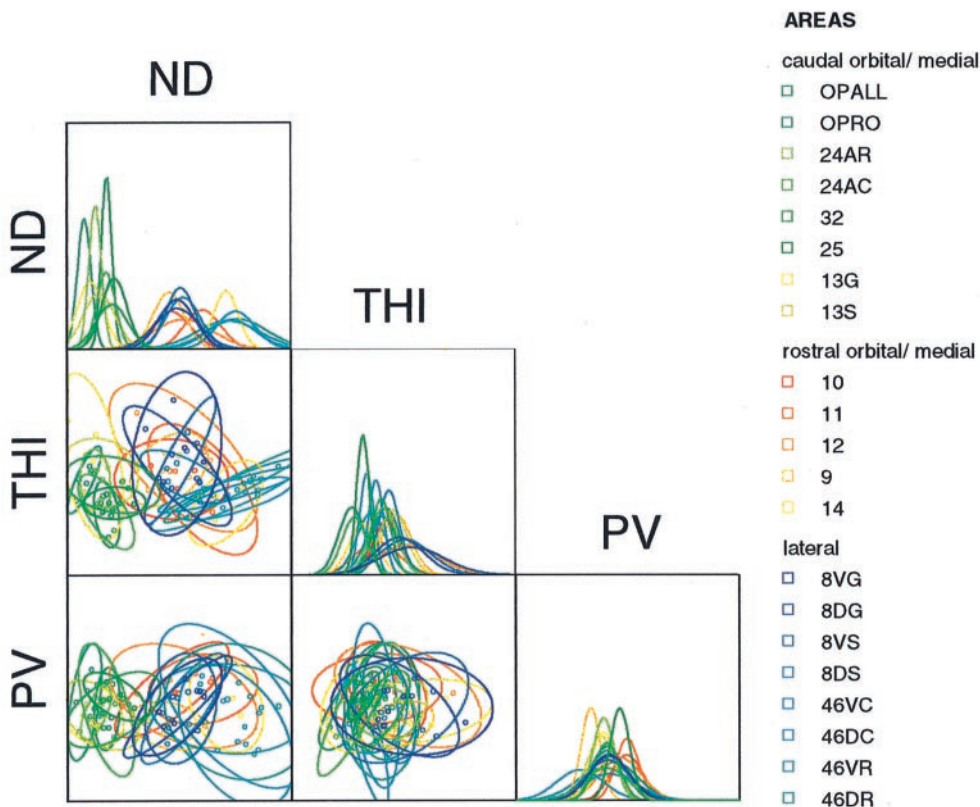


**Figure 8.** DA plot showing the separation of prefrontal areas for the three most informative experimental measures, ND, THI and PV staining. Diagram fields contain normal curves describing the distribution of individual data points for each area for single measures (e.g. ND × ND) and bivariate confidence ellipses for pairwise combinations of measures (e.g. ND × THI). Areas are colored according to their memberships in regional prefrontal groups: green to blue spectrum indicates caudal orbital and caudal medial areas (OPAll, OPro, 13 gyral and sulcal, and 24a rostral and caudal subdivisions, as well as areas 32 and 25); red or orange colors symbolize rostral orbital and medial areas (10, 11, O12, M9, M14); blue to green spectrum indicates lateral areas (all parts of areas 46 and 8). The clear separation particularly of ND measurements belonging to different areas is also borne out by the results of the DA described in Results.

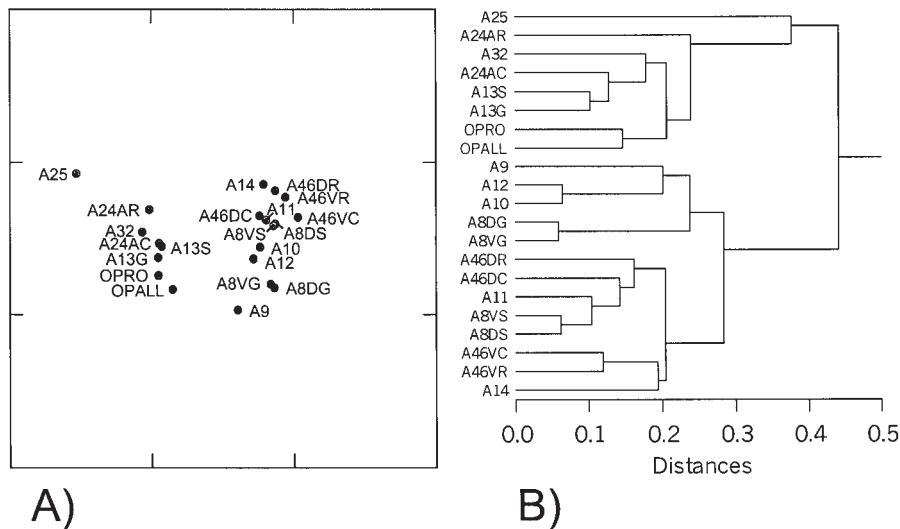


**Figure 9.** (A) NMDS plot indicating relative similarity of prefrontal areas according to their normalized laminar profiles across all experimental measures (ND, GD and THI for layers I, II–III and V–VI, and PV, CR and CB for layers I–III). The alienation coefficient for this configuration is 0.095. (B) Hierarchical cluster tree based on the (dis)similarity of normalized laminar profiles of prefrontal cortical areas using all experimental measures.

accordance with the outcome of the DA, all subsequent statistical analyses made use of the highly informative ND measure, combining it with information from other experimental variables, such as the THI and PV data.

#### Global Similarity of Areas Based on Different Experimental Measures

The NMDS plot in Figure 9A expresses the relative similarity of all prefrontal cortical areas in terms of their normalized laminar profiles for the combination of all experimental measures (ND, GD and THI for layers I, II–III and V–VI, and PV, CR and CB for layers I–III; layer IV information for ND, GD and THI as well as layer IV–VI information for PV, CR and CB was omitted owing to the normalization process described in Materials and Methods). Clearly apparent was the existence of two main groups, comprising granular areas on the one hand and agranular/dysgranular areas on the other, indicating a larger dissimilarity between the groups than within groups. Also apparent were some outliers, which were dissimilar from most other areas (most notably A25), as well as a sequential similarity structure within both groups of areas. The latter feature may hint on a regional organization along structural gradients. The tree shown in Figure 9B confirmed this global structure from the independent perspective of a hierarchical cluster analysis. It shows again the separation of all areas into two main groups and one very dissimilar outlier, area 25. The composition of the two main clusters once more followed the assignment of areas to an agranular/dysgranular group, on the one hand (at the top of the tree), and to a group of granular areas, on the other. The diagram also indicates a subdivision of the granular area group into gyral areas A8, A9, A10 and A12, and the remaining granular areas. Further, the organization of area 46 seems to follow mainly a ventral–dorsal divide, whereas area 8 appears to be split along sulcal and gyral subcomponents.

More detailed relationships became apparent when the two main groups of areas, that is, the granular and agranular/dysgranular areas, were each analyzed on their own (data not shown). These analyses confirmed the clear divide between the gyral and sulcal portions of A8 and the relative similarity

between at least the ventral subcomponents of area 46, and underlined the dissimilarity of area 25 from all other areas.

The initial impressions were confirmed when selected experimental measures, such as ND and THI, were combined for laminar areal profiles. The results (not shown) also suggested a similarity grouping of the gyral components of A8 and A9. The combined analysis of ND and PV variables for the laminar area profiles also validated the main prefrontal subdivisions, but additionally indicated a more gradual change in the areal profiles along these two measures. Such a gradient was borne out most clearly in the analyses of the relative laminar ND profiles on their own. The NMDS (not shown) indicated a striking one-dimensional similarity gradient from medial and orbital to rostral lateral and caudal lateral prefrontal cortices, when the areas were compared in the absence of information about layer IV. In this gradual distribution of profiles, however, some areas still appeared closely related (e.g. areas A25 and A14, areas A32 and A13, areas A46VC and A8V).

#### Discussion

##### Profiles of Prefrontal Areas Established by Cellular Density, PV and CB

Several findings emerged from this study. First, architectonic areas have distinct profiles that can be described quantitatively. The conventional and multidimensional analyses employed emphasized that among several cellular, laminar and molecular features, neuronal density was highly informative in establishing architectonic profiles, followed by cortical thickness and PV. Glial density, and CB were less informative, and CR not at all, as summarized in Figures 7, 8 and 10. Graphic representations from multidimensional analyses positioned areas along similarity–dissimilarity axes and demonstrated that there are graded architectonic differences in the prefrontal cortex, confirming and extending previous findings (Barbas and Pandya, 1989). Profiles thus established can be used to determine whether neighboring cortices are distinct or similar. These representations highlighted, for example, area 25 as distinct from its neighboring areas. In addition, area 46 appears to have several subdivisions, as noted in a recent study (Petrides and Pandya,

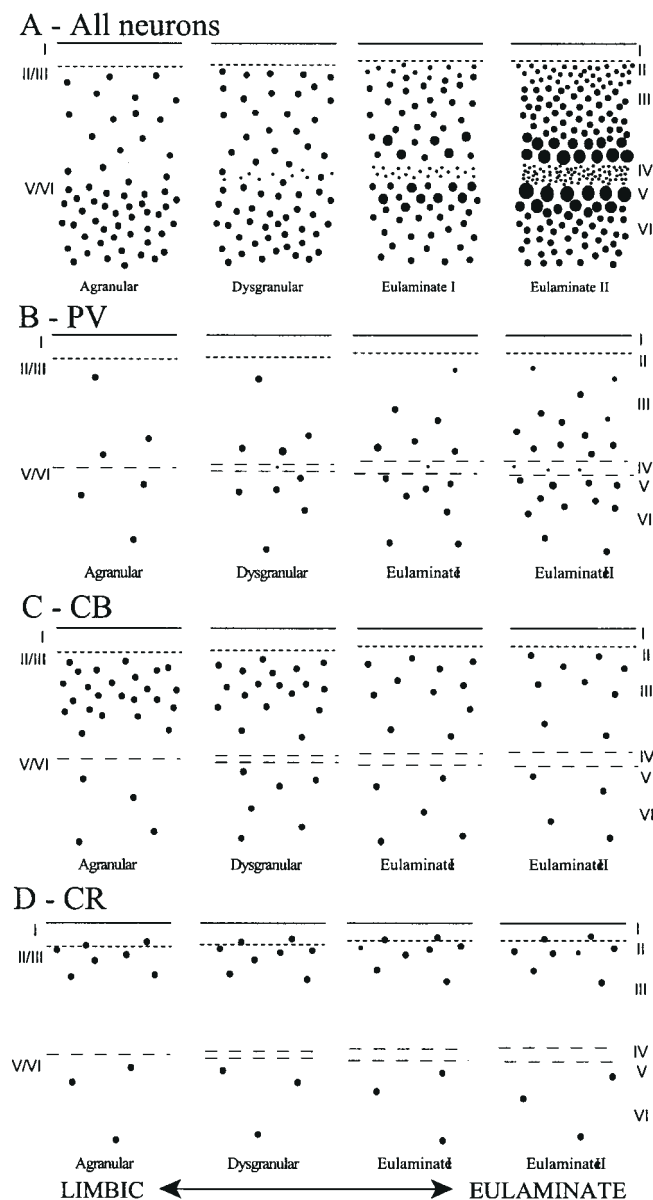


**Figure 10.** Sketch summarizing architectonic features by layer in different types of prefrontal cortices. (A) Neuronal density based on Nissl stain: agranular and dysgranular (limbic) areas have three or four layers, lack or have a rudimentary granular layer IV, and have the lowest density of neurons. Eulaminate I and II cortices have six layers, including a well defined and dense granular layer IV and the highest density of neurons. (B) PV positive neurons, found mostly in the central layers (III–V), were more prevalent in eulaminate cortices than in limbic cortices. (C) CB positive neurons, concentrated in the upper layers (II–III), were more prevalent in limbic cortices than in eulaminate cortices. (D) CR positive neurons were found mostly in the upper layers (I–III), and were evenly distributed among different types of prefrontal cortices.

1999), that may be related to their distinct roles in different aspects of working memory (Goldman-Rakic, 1996; Baddeley, 1996; Koehlin *et al.*, 1999).

These profiles may also help resolve differences in the maps published by various investigators. For example, the central/caudal orbitofrontal cortex was considered to be entirely within area 13 in the map of Walker (Walker, 1940), but was divided into three distinct areas (areas OPAII, OPro and 13) in another study (Barbas and Pandya, 1989). The present analyses suggest that even though caudal orbitofrontal areas have several features in common, their profiles differ significantly, suggesting that

they represent separate architectonic areas. Similarly, Walker named the region anterior to the upper limb of the arcuate sulcus area 8 (Walker, 1940), and the region anterior to the lower limb of the arcuate sulcus area 45, whereas Brodmann (Brodmann, 1905) considered both regions as part of area 8. The present analyses suggest that the anterior bank of both limbs of the arcuate sulcus has an overall lower density than the adjoining gyral cortex. This interesting deviation in cellular density may be consequent to differential forces exerted by axons establishing corticocortical connections [for discussion see (Scannell, 1997; Van Essen, 1997)].

Further to establishing the identity of each area, the present analyses demonstrated the relationship of each area to the rest, and suggest that architectonic areas can be grouped by common features. The most striking divide was between agranular/dysgranular (limbic) areas and eulaminate areas, on account of an overall lower cell density in limbic than in eulaminate areas, and a marked predominance in the number of neurons in the deep layers in comparison with the upper layers in limbic, but not in eulaminate, areas. Importantly, the differences appear to be systematic, since the prominence of the deep layers in limbic areas gave way to even distribution of neurons in the upper and deep layers in adjacent eulaminate I areas, and led to higher cell density in the upper layers in the best delineated eulaminate II cortices (Fig. 4). In this systematic sequence of laminar changes, granular layer IV was densest in eulaminate II areas, less dense in eulaminate I areas, rudimentary in dysgranular areas and absent in agranular areas. These systematic differences were accentuated by correlated differences in neurons positive for PV and CB, whose prevalence was comparable in eulaminate areas but lopsided in limbic cortices, where CB neurons outnumbered the PV by several-fold.

Further, the patterns we observed seem to extend to other cortices where laminar transitions have been identified, including the cingulate cortex of human and non-human primates (Zilles *et al.*, 1986; Vogt *et al.*, 1987, 1995; Hof and Nimchinsky, 1992; Nimchinsky *et al.*, 1997), entorhinal cortex (Amaral *et al.*, 1987; Tunon *et al.*, 1992; Insausti *et al.*, 1995; Mikkonen *et al.*, 1997), visual cortices (Leuba and Garey, 1989; Kondo *et al.*, 1999) and some prefrontal areas (Rajkowska and Goldman-Rakic, 1995; Gabbott and Bacon, 1996b). In all cases, the variations were concordant with differences in laminar definition in these areas [for a review see (Pandya *et al.*, 1988)].

#### Comparison with Related Studies

Detailed quantitative studies based on neuron counts and calcium binding proteins have previously been conducted for only a few prefrontal areas in a related primate species, *Macaca fascicularis* (Hendry *et al.*, 1987; Condé *et al.*, 1994; Gabbott and Bacon, 1996b). Neuronal density estimates for areas 24 and 25 in *M. mulatta* in this study are comparable to those reported by Gabbott and Bacon (Gabbott and Bacon, 1996b), who also used quantitative procedures, though our estimate for area 32 is lower. Similarly, our estimates for the density of CR and PV are comparable to their values, though our CB estimate is higher. The present data are also consistent with information provided in another study on the distribution of PV, CB and CR in areas 9, 46 and 11 (Condé *et al.*, 1994). Density estimates in the two studies appear to be comparable when converted to the same unit volume, at least for CB and PV, though their estimate for CR appears to be higher. Finally, our data are in agreement with differences in the prevalence of each of the calcium binding proteins (CBP) in different layers inside and outside the prefrontal cortex [e.g. (Condé *et al.*, 1994; Gabbott and Bacon,

1996b; Glezer *et al.*, 1998)]. Quantitative variations in different studies may be attributed to several factors, including species differences in the prefrontal cortex of *M. fascicularis* and *M. mulatta*, and technical factors, such as differential shrinkage of the brain, antibody penetration, among others. Finally, having sampled either exclusively dysgranular areas (Gabbott and Bacon, 1996b) or exclusively eulaminate areas (Condé *et al.*, 1994) using conventional statistics, no major regional differences were noted in the above studies.

### ***The Cellular and Molecular Features of Different Types of Prefrontal Cortices May Have Their Roots in Development***

How do the specific cellular and molecular features arise in different types of prefrontal cortices? The pattern of cellular proliferation, cell cycle duration, migration and neuronal elimination have fundamental roles in shaping the cortex [for reviews see (Sidman and Rakic, 1973; McConnell, 1991; Finlay and Darlington, 1995; Caviness *et al.*, 1995)] and may account for the distinct laminar profiles of limbic and eulaminate areas seen here. According to the estimates of Caviness *et al.* (Caviness *et al.*, 1995), in early cortical development cell cycle duration is longer and fewer cells migrate to the cortex, suggesting that the least densely populated limbic areas may complete their development before eulaminate areas. Our data also indicate that while cellular density was approximately equal in the deep layers in all prefrontal areas, there was a bias in the upper layers across areas, where the limbic areas were impoverished in comparison with the eulaminate ones. This evidence is consistent with a uniform onset of development of the cortex, in general, as suggested by Rakic *et al.* (Rakic *et al.*, 1986), and further suggests that the developmental epoch may be prolonged in eulaminate areas. The higher overall density in eulaminate areas can be explained by a higher density in layers IV, III and II, which are formed after the deep layers, according to the inside-out pattern of development of the cortex [for a review see (Rakic, 1988)]. Our data suggest that neuronal migration may be particularly prolonged for lateral areas 46 and 8, affecting the upper layers (II and III), consistent with their formation at a time when more neurons migrate to the cortex (Caviness *et al.*, 1995). In addition, CB, which is found in abundance in limbic areas, shows a high level of expression in early prenatal development, and is significantly reduced during cortical maturation in primates (Hendrickson *et al.*, 1991; Cao *et al.*, 1996; Yan *et al.*, 1997). In contrast, the prevalence of PV positive neurons is low during early development and high during postnatal maturation (Hendrickson *et al.*, 1991; Cao *et al.*, 1996; Letinic and Kostovic, 1998). Differential elimination of neurons during development may be an additional important process in sculpting the cortex [e.g. (Finlay and Slattery, 1983)].

### ***Functional Implications***

The cellular and neurochemical distinction of eulaminate from limbic cortices has several implications for function. While the density of glia was similar among prefrontal cortices, in agreement with other studies (Garey and Leuba, 1986; Leuba and Garey, 1989), agranular limbic areas had a higher ratio of glia to neurons than the eulaminate areas. A high ratio of glia to neurons has been associated with increased neuronal activity (Diamond *et al.*, 1966; Szeligo and Leblond, 1977). In fact, agranular limbic areas have widespread connections and may exercise a tonic influence on the neuraxis [for a review see (Barbas, 1995)].

### ***CB and PV May Preferentially Mark Parallel Cortical Systems***

The differential distribution of CB and PV in prefrontal cortices is reminiscent of their preferential expression in two functionally distinct thalamic systems [for a review see (Jones, 1998)]. In sensory relay nuclei of the thalamus, CB positive neurons constitute a distributed thalamocortical system projecting widely to the superficial cortical layers (Jones, 1998). In contrast, PV positive neurons are prevalent in topographically specific sensory thalamic nuclei that project selectively to the middle layers of the cortex (Jones, 1998). Unlike the thalamus, however, where CB and PV are expressed in projection neurons, in the cortex they label mostly, though not exclusively, interneurons [for reviews see (Jones, 1993; DeFelipe, 1997)]. The best delineated eulaminate cortices project predominantly to the middle and deep layers of other cortices, like thalamic neurons that express PV. In contrast, limbic cortices, which are enriched in CB positive neurons, issue widespread projections terminating mostly in the superficial layers of eulaminate cortices (Barbas and Rempel-Clower, 1997), akin to the thalamic neurons that express CB (Jones, 1998).

It is generally accepted that CB labels pyramidal neurons in the cortex as well [for reviews see (DeFelipe, 1997; Hof *et al.*, 1999)]. Moreover, whereas the distribution of non-pyramidal CB positive neurons appears to be uniform among occipitotemporal cortices, the prevalence of CB positive pyramidal neurons varies widely, ranging from 5–10% in sensory association cortices to ~50% of the total number in anterior temporal limbic cortices (Kondo *et al.*, 1999). The preponderance of CB positive neurons in prefrontal limbic areas is consistent with the latter study. Further studies are necessary to determine whether some CB positive pyramidal neurons in prefrontal limbic areas are projection neurons.

### ***Prefrontal Architecture and Implications for Neuropathology***

While prefrontal limbic and eulaminate cortices are similar in the prevalence of neurons with CBP in the upper layers, they differ markedly in their mode of connection (Barbas, 1986; Barbas and Rempel-Clower, 1997; Rempel-Clower and Barbas, 2000). In limbic areas the deep layers are the principal sources and targets of corticocortical connections, whereas in eulaminate areas it is the upper layers that primarily issue and receive cortical connections (Barbas and Rempel-Clower, 1997). This evidence suggests that activity levels and CBP are matched in eulaminate cortices, but are notably mismatched in limbic areas. The functional significance of this finding is based on the putative role of neurons with CBP to sequester, buffer and transport intracellular calcium [for reviews see (Baimbridge *et al.*, 1992; Heizmann, 1992)], essential processes for balancing excitation through inhibitory control (Sloviter, 1989; Freund *et al.*, 1990; Sloviter *et al.*, 1991). Neurons positive for PV, CB and CR represent distinct subclasses of GABAergic interneurons in the cortex and may have a powerful inhibitory control on local circuits (Celio *et al.*, 1986; DeFelipe *et al.*, 1989; Hendry *et al.*, 1989; Celio, 1990; Lewis and Lund, 1990; Hof and Nimchinsky, 1992; Williams *et al.*, 1992; Lund and Lewis, 1993; Condé *et al.*, 1994; Gabbott and Bacon, 1996a). The mismatch in the focus of connections and prevalence of inhibitory neurons that have CBP and the capacity to buffer and sequester calcium may provide a clue as to why limbic areas have a predilection for epileptiform activity (Penfield and Jasper, 1954).

The role of calcium binding proteins, however, is not restricted to calcium regulation, but extends to a wide variety of cellular activities, including cytoskeletal organization, cell cycle regulation and plasticity [for reviews see (Kater *et al.*,

1988; Heizmann, 1992)]. CB positive neurons appear to be preferentially affected in several cortical areas in patients with Alzheimer's disease (Ichimiya *et al.*, 1988; Nishiyama *et al.*, 1993) or frontal lobe dementia (Ferrer *et al.*, 1993). Limbic areas, which have the highest proportion of CB positive neurons, are the most severely affected in Alzheimer's disease (Hooper and Vogel, 1976; Hyman *et al.*, 1984; Van Hoesen and Hyman, 1990; Vogt *et al.*, 1990). In contrast, neurons positive for CR, which show a more uniform distribution in the prefrontal cortex, are unaffected in Alzheimer's disease (Hof *et al.*, 1993; Fonseca and Soriano, 1995; Leuba *et al.*, 1998). In addition, in lateral prefrontal areas of schizophrenic patients the density of CB positive neurons is greater than in normal controls (Daviss and Lewis, 1995), as is the overall neuronal density (Selemon *et al.*, 1998).

In summary, prefrontal limbic and eulaminate cortices have distinct cellular and molecular features that may contribute to their distinct role in cognition, memory and emotions [for a review see (Barbas, 2000)]. Further studies are necessary to determine whether different types of prefrontal cortices develop at a different rate, since that would render them vulnerable to insults occurring at different developmental epochs, and may help explain the varied symptomatology in diseases which have their roots in development, including schizophrenia, learning disabilities and some forms of epilepsy.

## Notes

This work was supported by grants NS24760 (NINDS) and NS57414 (NIMH).

Address correspondence to H. Barbas, Boston University, 635 Commonwealth Ave., Room 431, Boston, MA 02215, USA. Email: barbas@bu.edu.

## References

Amaral DG, Insausti R, Cowan WM (1987) The entorhinal cortex of the monkey. I. Cytoarchitectonic organization. *J Comp Neurol* 264:326-355.

Baddeley A (1996) The fractionation of working memory. *Proc Natl Acad Sci USA* 93:13468-13472.

Baimbridge KG, Celio MR, Rogers JH (1992) Calcium-binding proteins in the nervous system. *Trends Neurosci* 15:303-308.

Barbas H (1986) Pattern in the laminar origin of corticocortical connections. *J Comp Neurol* 252:415-422.

Barbas H (1995) Anatomic basis of cognitive-emotional interactions in the primate prefrontal cortex. *Neurosci Biobehav Rev* 19:499-510.

Barbas H (2000) Connections underlying the synthesis of cognition, memory, and emotion in primate prefrontal cortices. *Brain Res Bull* 52:319-330.

Barbas H, Pandya DN (1989) Architecture and intrinsic connections of the prefrontal cortex in the rhesus monkey. *J Comp Neurol* 286:353-375.

Barbas H, Rempel-Clover N (1997) Cortical structure predicts the pattern of corticocortical connections. *Cereb Cortex* 7:635-646.

Barbas H, Ghashghaei H, Dombrowski SM, Rempel-Clover NL (1999) Medial prefrontal cortices are unified by common connections with superior temporal cortices and distinguished by input from memory-related areas in the rhesus monkey. *J Comp Neurol* 410:343-367.

Braendgaard H, Gundersen HJG (1986) The impact of recent stereological advances on quantitative studies of the nervous system. *J Neurosci Methods* 18:39-78.

Brodmann K (1905) Beiträge zur histologischen Lokalisation der Grosshirnrinde. III. Mitteilung: Die Rindenfelder der niederen Affen. *J Psychol Neurol* 4:177-266.

Cao QL, Yan XX, Luo XG, Garey LJ (1996) Prenatal development of parvalbumin immunoreactivity in the human striate cortex. *Cereb Cortex* 6:620-630.

Carmichael ST, Price JL (1994) Architectonic subdivision of the orbital and medial prefrontal cortex in the macaque monkey. *J Comp Neurol* 346:366-402.

Caviness VS, Jr., Takahashi T, Nowakowski RS (1995) Numbers, time and

neocortical neuronogenesis: a general developmental and evolutionary model. *Trends Neurosci* 18:379-383.

Celio MR (1990) Calbindin D-28k and parvalbumin in the rat nervous system. *Neurosci* 35:375-475.

Celio MR, Scharer L, Morrison JH, Norman AW, Bloom FE (1986) Calbindin immunoreactivity alternates with cytochrome c-oxidase-rich zones in some layers of the primate visual cortex. *Nature* 323:715-717.

Celio MR, Baier W, Scharer L, de Viragh PA, Gerday C (1988) Monoclonal antibodies directed against the calcium binding protein parvalbumin. *Cell Calcium* 9:81-86.

Celio MR, Baier W, Scharer L, Gregersen HJ, de Viragh PA, Norman AW (1990) Monoclonal antibodies directed against the calcium binding protein calbindin D-28k. *Cell Calcium* 11:599-602.

Coggeshall RE, Lekan HA (1996) Methods of determining numbers of cells and synapses: a case for more uniform standards of review. *J Comp Neurol* 364:6-15.

Condé F, Lund JS, Jacobowitz DM, Baimbridge KG, Lewis DA (1994) Local circuit neurons immunoreactive for calretinin, calbindin D-28k or parvalbumin in monkey prefrontal cortex: distribution and morphology. *J Comp Neurol* 341:95-116.

Daviss SR, Lewis DA (1995) Local circuit neurons of the prefrontal cortex in schizophrenia: selective increase in the density of calbindin-immunoreactive neurons. *Psychiatr Res* 59:81-96.

DeFelipe J (1997) Types of neurons, synaptic connections and chemical characteristics of cells immunoreactive for calbindin-D28K, parvalbumin and calretinin in the neocortex. *J Chem Neuroanat* 14:1-19.

DeFelipe J, Hendry SH, Jones EG (1989) Visualization of chandelier cell axons by parvalbumin immunoreactivity in monkey cerebral cortex. *Proc Natl Acad Sci USA* 86:2093-2097.

Diamond MC, Law F, Rhodes H, Lindner B, Rosenzweig MR, Krech D, Bennett EL (1966) Increases in cortical depth and glia numbers in rats subjected to enriched environment. *J Comp Neurol* 128:117-126.

Ferrer I, Tunon T, Serrano MT, Casas R, Alcantara S, Zujar MJ, Rivera RM (1993) Calbindin D-28k and parvalbumin immunoreactivity in the frontal cortex in patients with frontal lobe dementia of non-Alzheimer type associated with amyotrophic lateral sclerosis. *J Neurol Neurosurg Psychiatr* 56:257-261.

Finlay BL, Darlington RB (1995) Linked regularities in the development and evolution of mammalian brains. *Science* 268:1578-1583.

Finlay BL, Slattery M (1983) Local differences in the amount of early cell death in neocortex predict adult local specializations. *Science* 219:1349-1351.

Fonseca M, Soriano E (1995) Calretinin-immunoreactive neurons in the normal human temporal cortex and in Alzheimer's disease. *Brain Res* 691:83-91.

Freund TF, Buzsaki G, Leon A, Baimbridge KG, Somogyi P (1990) Relationship of neuronal vulnerability and calcium binding protein immunoreactivity in ischemia. *Exp Brain Res* 83:55-66.

Fuster JM (1989) The prefrontal cortex. New York: Raven Press.

Fuster JM (1993) Frontal lobes. *Curr Opin Neurobiol* 3:160-165.

Gabbott PL, Bacon SJ (1996a) Local circuit neurons in the medial prefrontal cortex (areas 24a, b,c, 25 and 32) in the monkey. I. Cell morphology and morphometrics. *J Comp Neurol* 364:567-608.

Gabbott PL, Bacon SJ (1996b) Local circuit neurons in the medial prefrontal cortex (areas 24a, b,c, 25 and 32) in the monkey. II. Quantitative areal and laminar distributions. *J Comp Neurol* 364:609-636.

Gabbott PL, Stewart MG (1987) Distribution of neurons and glia in the visual cortex (area 17) of the adult albino rat: a quantitative description. *Neuroscience* 21:833-845.

Garey LJ, Leuba G (1986) A quantitative study of neuronal and glial numerical density in the visual cortex of the bottlenose dolphin: evidence for a specialized subarea and changes with age. *J Comp Neurol* 247:491-496.

Glezer II, Hof PR, Morgane PJ (1998) Comparative analysis of calcium-binding protein-immunoreactive neuronal populations in the auditory and visual systems of the bottlenose dolphin (*Tursiops truncatus*) and the macaque monkey (*Macaca fascicularis*). *J Chem Neuroanat* 15:203-237.

Goldman-Rakic PS (1988) Topography of cognition: parallel distributed networks in primate association cortex. *Annu Rev Neurosci* 11:137-156.

Goldman-Rakic PS (1996) Regional and cellular fractionation of working memory. *Proc Natl Acad Sci USA* 93:13473-13480.

- Gonchar Y, Burkhalter A (1997) Three distinct families of GABAergic neurons in rat visual cortex. *Cereb Cortex* 7:347-358.
- Gundersen HJG, Bagger P, Bendtsen TF, Evans SM, Korbo L, Marcussen N, Moller A, Nielsen K, Nyengaard JR, Pakkenberg B, Sorensen FB, Vesterby A, West MJ (1988) The new stereological tools: disector, fractionator, nucleator and point sample intercepts and their use in pathological research and diagnosis. *APMIS* 96:857-881.
- Guttman L (1968) A general nonmetric technique for finding the smallest coordinate space for a configuration of points. *Psychometrika* 33: 469-506.
- Heizmann CW (1992) Calcium-binding proteins: basic concepts and clinical implications. *Gen Physiol Biophys* 11:411-425.
- Hendrickson AE, Van Brederode JFM, Mulligan KA, Celio MR (1991) Development of the calcium-binding proteins parvalbumin and calbindin in monkey striate cortex. *J Comp Neurol* 307:626-646.
- Hendry SHC, Schwark HD, Jones EG, Yan J (1987) Numbers and proportions of GABA-immunoreactive neurons in different areas of monkey cerebral cortex. *J Neurosci* 7:1503-1519.
- Hendry SHC, Jones EG, Emson PC, Lawson DEM, Heizmann CW, Streit P (1989) Two classes of cortical GABA neurons defined by differential calcium binding protein immunoreactivities. *Exp Brain Res* 76: 467-472.
- Hof PR, Nimchinsky EA (1992) Regional distribution of neurofilament and calcium-binding proteins in the cingulate cortex of the macaque monkey. *Cereb Cortex* 2:456-467.
- Hof PR, Nimchinsky EA, Celio MR, Bouras C, Morrison JH (1993) Calretinin-immunoreactive neocortical interneurons are unaffected in Alzheimer's disease. *Neurosci Lett* 152:145-148.
- Hof PR, Glezer II, Condé F, Flagg RA, Rubin MB, Nimchinsky EA, Vogt Weisenhorn DM (1999) Cellular distribution of the calcium-binding proteins parvalbumin, calbindin, and calretinin in the neocortex of mammals: phylogenetic and developmental patterns. *J Chem Neuroanat* 16:77-116.
- Hooper MW, Vogel FS (1976) The limbic system in Alzheimer's disease. *Am J Pathol* 85:1-20.
- Hyman BT, Van Hoesen GW, Damasio AR, Barnes CL (1984) Alzheimer's disease: cell-specific pathology isolates the hippocampal formation. *Science* 225:1168-1170.
- Ichimiyama Y, Emson PC, Mountjoy CQ, Lawson DE, Heizmann CW (1988) Loss of calbindin-28K immunoreactive neurons from the cortex in Alzheimer-type dementia. *Brain Res* 475:156-159.
- Insausti R, Tunón T, Sobreviela T, Insausti AM, Gonzalo LM (1995) The human entorhinal cortex: a cytoarchitectonic analysis. *J Comp Neurol* 355:171-198.
- Jones EG (1993) GABAergic neurons and their role in cortical plasticity in primates. *Cereb Cortex* 3:361-372.
- Jones EG (1998) Viewpoint: the core and matrix of thalamic organization. *Neurosci* 85:331-345.
- Jones EG, Dell'Anna ME, Molinari M, Rausell E, Hashikawa T (1995) Subdivisions of macaque monkey auditory cortex revealed by calcium-binding protein immunoreactivity. *J Comp Neurol* 362:153-170.
- Kater SB, Mattson MP, Cohan C, Connor J (1988) Calcium regulation of the neuronal growth cone. *Trends Neurosci* 11:315-321.
- Koechlin E, Basso G, Pietrini P, Panzer S, Grafman J (1999) The role of the anterior prefrontal cortex in human cognition. *Nature* 399:148-151.
- Kondo H, Tanaka K, Hashikawa T, Jones EG (1999) Neurochemical gradients along monkey sensory cortical pathways: calbindin-immunoreactive pyramidal neurons in layers II and III. *Eur J Neurosci* 11:4197-4203.
- Kruskal JB (1964) Multidimensional scaling by optimizing goodness of fit to a nonmetric hypothesis. *Psychometrika* 29:1-27.
- Kubota Y, Hattori R, Yui Y (1994) Three distinct subpopulations of GABAergic neurons in rat frontal agranular cortex. *Brain Res* 649: 159-173.
- Letinic K, Kostovic I (1998) Postnatal development of calcium-binding proteins calbindin and parvalbumin in human visual cortex. *Cereb Cortex* 8:660-669.
- Leuba G, Garey IJ (1989) Comparison of neuronal and glial numerical density in primary and secondary visual cortex of man. *Exp Brain Res* 77:31-38.
- Leuba G, Kraftsik R, Saini K (1998) Quantitative distribution of parvalbumin, calretinin, and calbindin D-28k immunoreactive neurons in the visual cortex of normal and Alzheimer cases. *Exp Neurol* 152: 278-291.
- Lewis DA, Lund JS (1990) Heterogeneity of chandelier neurons in monkey neocortex: corticotropin-releasing factor- and parvalbumin-immunoreactive populations. *J Comp Neurol* 293:599-615.
- Ling EA, Leblond CP (1973) Investigation of glial cells in semithin sections. II. Variation with age in the numbers of the various glial cell types in rat cortex and corpus callosum. *J Comp Neurol* 149:73-81.
- Ling EA, Paterson JA, Privat A, Mori S, Leblond CP (1973) Investigation of glial cells in semithin sections. I. Identification of glial cells in the brain of young rats. *J Comp Neurol* 149:43-71.
- Lund JS, Lewis DA (1993) Local circuit neurons of developing and mature macaque prefrontal cortex: Golgi and immunocytochemical characteristics. *J Comp Neurol* 328:282-312.
- McConnell SK (1991) The generation of neuronal diversity in the central nervous system. *Annu Rev Neurosci* 14:269-300.
- Mikkonen M, Soinen H, Pitkanen A (1997) Distribution of parvalbumin-, calretinin-, and calbindin-D28k-immunoreactive neurons and fibers in the human entorhinal cortex. *J Comp Neurol* 388:64-88.
- Morecraft RJ, Geula C, Mesulam M-M (1992) Cytoarchitecture and neural afferents of orbitofrontal cortex in the brain of the monkey. *J Comp Neurol* 323:341-358.
- Nimchinsky EA, Hof PR, Young WG, Morrison JH (1996) Neurochemical, morphologic, and laminar characterization of cortical projection neurons in the cingulate motor areas of the macaque monkey. *J Comp Neurol* 374:136-160.
- Nimchinsky EA, Vogt BA, Morrison JH, Hof PR (1997) Neurofilament and calcium-binding proteins in the human cingulate cortex. *J Comp Neurol* 384:597-620.
- Nishiyama E, Ohwada J, Iwamoto N, Arai H (1993) Selective loss of calbindin D28K-immunoreactive neurons in the cortical layer II in brains of Alzheimer's disease: a morphometric study. *Neurosci Lett* 163:223-226.
- O'Kusky J, Colonnier M (1982) A laminar analysis of the number of neurons, glia, and synapses in the visual cortex (area 17) of adult macaque monkeys. *J Comp Neurol* 210:278-290.
- Pandya DN, Seltzer B, Barbas H (1988) Input-output organization of the primate cerebral cortex. In: *Comparative primate biology*, Vol. 4. Neurosciences (Steklis HD, Erwin J, eds), pp. 39-80. New York: Alan R. Liss.
- Penfield W, Jasper H (1954) *Epilepsy and the functional anatomy of the human brain*. Boston, MA: Little, Brown & Company.
- Petrides M (1989) Frontal lobes and memory. In: *Handbook of Neuropsychology*, Vol. 3. Memory and its disorders (Boller F, Grafman J, eds), pp. 75-90. New York: Elsevier Science Publishers B.V.
- Petrides M, Pandya DN (1999) Dorsolateral prefrontal cortex: comparative cytoarchitectonic analysis in the human and the macaque brain and corticocortical connection patterns. *Eur J Neurosci* 11: 1011-1036.
- Preuss TM, Goldman-Rakic PS (1991) Myelo- and cytoarchitecture of the granular frontal cortex and surrounding regions in the strepsirrhine primate *Galago* and the anthropoid primate *Macaca*. *J Comp Neurol* 310:429-474.
- Rajkowska G, Goldman-Rakic PS (1995) Cytoarchitectonic definition of prefrontal areas in the normal human cortex. I. Remapping of areas 9 and 46 using quantitative criteria. *Cereb Cortex* 5:307-322.
- Rakic P (1988) Specification of cerebral cortical areas. *Science* 241: 170-176.
- Rakic P, Bourgeois JP, Eckenhoff MF, Zecevic N, Goldman-Rakic PS (1986) Concurrent overproduction of synapses in diverse regions of the primate cerebral cortex. *Science* 232:232-235.
- Rempel-Clower NL, Barbas H (2000) The laminar pattern of connections between prefrontal and anterior temporal cortices in the Rhesus monkey is related to cortical structure and function. *Cereb Cortex* 10:851-865.
- Rosene DL, Rhodes KJ (1990) Cryoprotection and freezing methods that control ice crystal artifact and frozen sections from fixed and unfixed blocks of monkey and human brain tissue. In: *Handbook of Neuroscience Methods* 3. Quantitative and qualitative microscopy (Conn PM, ed.), pp. 360-385. New York: Academic Press.
- Sanides F (1970) Functional architecture of motor and sensory cortices in primates in the light of a new concept of neocortex evolution. In: *The primate brain: advances in primatology* (Noback CR, Montagna W, eds), pp. 137-208. New York: Appleton-Century-Crofts.
- Scannell JW (1997) Determining cortical landscapes. *Nature* 386:452.
- Schwaller B, Buchwald P, Blumcke I, Celio MR, Hunziker W (1993) Characterization of a polyclonal antiserum against the purified

- human recombinant calcium binding protein calretinin. *Cell Calcium* 14:639-648.
- Selemon LD, Rajkowska G, Goldman-Rakic PS (1995) Abnormally high neuronal density in the schizophrenic cortex. A morphometric analysis of prefrontal area 9 and occipital area 17. *Arch Gen Psychiatry* 52:805-18.
- Selemon LD, Rajkowska G, Goldman-Rakic PS (1998) Elevated neuronal density in prefrontal area 46 in brains from schizophrenic patients: application of a three-dimensional, stereologic counting method. *J Comp Neurol* 392:402-412.
- Sidman RL, Rakic P (1973) Neuronal migration, with special reference to developing human brain: a review. *Brain Res* 62:1-35.
- Sloviter RS (1989) Calcium-binding protein (calbindin-D28k) and parvalbumin immunocytochemistry: localization in the rat hippocampus with specific reference to the selective vulnerability of hippocampal neurons to seizure activity. *J Comp Neurol* 280:183-196.
- Sloviter RS, Sollas AL, Barbaro NM, Laxer KD (1991) Calcium-binding protein (calbindin-D28K) and parvalbumin immunocytochemistry in the normal and epileptic human hippocampus. *J Comp Neurol* 308:381-396.
- Stephan KE, Zilles K, Kötter R (2000) Coordinate-independent mapping of structural and functional data by objective relational transformation (ORT). *Phil Trans R Soc Lond B Biol Sci* 355:37-54.
- Sterio DC (1984) The unbiased estimation of number and sizes of arbitrary particles using the disector. *J Microsc* 134:127-136.
- Szeligo F, Leblond CP (1977) Response of the three main types of glial cells of cortex and corpus callosum in rats handled during suckling or exposed to enriched, control and impoverished environments following weaning. *J Comp Neurol* 172:247-263.
- Tunon T, Insausti R, Ferrer I, Sobreviela T, Soriano E (1992) Parvalbumin and calbindin D-28K in the human entorhinal cortex. An immunohistochemical study. *Brain Res* 589:24-32.
- van Brederode JF, Mulligan KA, Hendrickson AE (1990) Calcium-binding proteins as markers for subpopulations of GABAergic neurons in monkey striate cortex. *J Comp Neurol* 298:1-22.
- Van Essen DC (1997) A tension-based theory of morphogenesis and compact wiring in the central nervous system. *Nature* 385:313-318.
- Van Hoesen GW, Hyman BT (1990) Hippocampal formation: anatomy and the patterns of pathology in Alzheimer's disease. *Prog Brain Res* 83:445-457.
- Vogt C, Vogt O (1919) Die physiologische Bedeutung der architektonischen Rindenfelderung auf Grund neuer Rindenreizungen. *J Psychol Neurol* 25:399-429.
- Vogt BA, Pandya DN, Rosene DL (1987) Cingulate cortex of the rhesus monkey. I. Cytoarchitecture and thalamic afferents. *J Comp Neurol* 262:256-270.
- Vogt BA, Van Hoesen GW, Vogt LJ (1990) Laminar distribution of neuron degeneration in posterior cingulate cortex in Alzheimer's disease. *Acta Neuropathol (Berl)* 80:581-589.
- Vogt BA, Nimchinsky EA, Vogt LJ, Hof PR (1995) Human cingulate cortex: surface features, flat maps, and cytoarchitecture. *J Comp Neurol* 359:490-506.
- Von Bonin G, Bailey P (1947) The neocortex of *Macaca mulatta*. Urbana, IL: University of Illinois Press.
- Walker AE (1940) A cytoarchitectural study of the prefrontal area of the macaque monkey. *J Comp Neurol* 73:59-86.
- West MJ (1993) New stereological methods for counting neurons. *Neurobiol Aging* 14:275-285.
- West MJ, Gundersen HJG (1990) Unbiased stereological estimation of the number of neurons in the human hippocampus. *J Comp Neurol* 296:1-22.
- West MJ, Slomianka L, Gundersen HJG (1991) Unbiased stereological estimation of the total number of neurons in the subdivisions of the rat hippocampus using the optical fractionator. *Anat Rec* 231:482-497.
- Williams RW, Rakic P (1988) Three-dimensional counting: an accurate and direct method to estimate numbers of cells in sectioned material. *J Comp Neurol* 278:344-352.
- Williams SM, Goldman-Rakic PS, Leranth C (1992) The synaptology of parvalbumin-immunoreactive neurons in the primate prefrontal cortex. *J Comp Neurol* 320:353-369.
- Yan XX, Cao QL, Luo XG, Garey LJ (1997) Prenatal development of calbindin D-28K in human visual cortex. *Cereb Cortex* 7:57-62.
- Zilles K, Armstrong E, Schlaug G, Schleicher A (1986) Quantitative cytoarchitectonics of the posterior cingulate cortex in primates. *J Comp Neurol* 253:514-524.